Adaptive Droop Controller for a Hybrid 375Vdc/48Vdc/400Vac AC/DC Microgrid

Carlos Gómez-Aleixandre, Ángel Navarro-Rodríguez, Geber Villa, Cristian Blanco and Pablo García
Dept. of Electrical, Electronics, Systems & Computers Engineering
University of Oviedo, LEMUR Group
Gijón, 33204, Spain
Email: gomeztcarlos@uniovi.es, navarroangel@uniovi.es, villageber@uniovi.es,
blancocristian@uniovi.es, garciafpablo@uniovi.es

***Abstract*—This paper studies the sharing control scheme for a Hybrid 48V/375V/400Vac AC/DC Microgrid, based on classical droop control and a novel approach for secondary control. In this paper, both the dc and ac grids are controlled by a P/V droop strategy. At the ac grid, this assumes a main resistive component in the distribution line impedance. The droop control voltage error in steady state is compensated by a novel and simple secondary control approach. The proposed control strategy is based on the calculation of the optimum power flow in each operating point and the real-time modification of the droop characteristics of the converters involved in the power flow calculation. The proposed control is also capable of eliminating the induced voltage drop when using virtual impedance and incorporating any power sharing criteria for the converters contributing to the power production, being this flexibility one of its more important characteristics.**

***Index Terms*—Microgrids, hybrid power systems, secondary control, voltage control, load flow control.**

I. Introduction

The future electricity grid is gradually moving in the direction of dc distribution, due the envisaged lower distribution losses (compared with ac distribution) and the more efficient integration of renewables and distributed resources [1]–[3]. The evolution in power electronics and control technologies has enabled the development of dc Low-Voltage (LV) microgrids, which eases the integration of Energy Storage Systems (ESS). Although the pathway from traditional ac distribution systems to these new topologies integrating is not clear, it is reasonable to think that the new grids should take advantage of the already existing ac infrastructure, leading to the creation of hybrid ac/dc microgrids [1]. This hybrid approach should use Power Electronic Converters (PEC) in order to provide redundancy of power flows, thus increasing the grid resiliency [4].

Droop techniques are a widely used control strategy to coordinate PECs so that they can share power production. In dc, P/V droop is used, as well as for ac in LV distribution levels, due to the fact that the grid impedance in LV networks is mainly resistive [5]. Droop techniques cause a deviation from nominal values for the variables involved. In the case of P/V droop, a deviation from nominal voltage appears due to the droop operation. Apart from that,for the P/V droop, the active power sharing among the converters is not always accurate, as the converters normally see different voltages. This is the same that happens for reactive power in Q/V droop.

Secondary control is used to eliminate voltage deviation due to the droop. Secondary control typically relies on integrators or PI regulators to eliminate the voltage deviation, both in ac [6] and dc [7]. This requires periodic calculations for the integrator to operate, gradually reducing the error every cycle.

This type of secondary control is normally divided into three categories: centralized, distributed and decentralized [8]. Centralized control has a central controller with communications with the control of each involved converter and measures the area voltage in order to eliminate its deviation, normally with a PI regulator, sending the same reference to all the converters. Distributed control operates in a similar way, but the PI regulator is implemented on each converter control, but with communication among all the converters. Decentralized control does not require neither central controller nor communications.

Secondary control can also be used to achieve accurate power sharing in P/V droops [9]. However, these methods add some extra complexity to the secondary control, with an extra control loop with a PI regulator and they are not suitable for decentralized secondary control, since they use some communication between PECs.

This paper shows a proposal of a hybrid ac/dc microgrid and the coordinated control of all the involved converters (ac/dc and dc/dc). The coordinated control is composed of a P/V droop control for the primary control and a novel approach for the secondary control. The proposed secondary control is applied to P/V droop, but it could be easily adapted to P/f+Q/V droop or other alternatives.

The proposed secondary control is able to eliminate the voltage deviation due to droop controllers based on a single calculation of the optimum power flow, shifting the droop characteristic of each converter according to voltage and power obtained from the power flow. This proposed solution has

The present work has been partially supported by the predoctoral grants program FPU for the formation in university teaching of Spain MECD under the grant IDs FPU16/05313 and FPU16/06829. This work also was supported in part by Spanish Ministry of Science and Innovation under grant MCI-20-PID2019-111051RB-I00 and the European Union's H2020 Research and Innovation programme under Grant Agreement No 864459 (UE-19-TALENT-864459).

TABLE I
COMPARISON BETWEEN THE PROPOSED SECONDARY CONTROL AND ALTERNATIVES IN THE LITERATURE BASED ON PI REGULATORS [8].

	Central controller required	Communication required	Robustness against data loss, communication delays or high latency	Power sharing accuracy	Flexibility to change the power sharing
Proposed	Yes	Yes	High	Yes	Yes
Centralized	Yes	Yes	Low	Extra PI reg.	No
Distributed	No	Yes	Medium	Extra PI reg.	No
Decentralized	No	No	Complete (no communication)	No	No

two main advantages compared to the aforementioned ones (centralized, distributed and decentralized).

Firstly, it is capable of achieving power sharing accuracy for the P/V droop without extra complexity. Besides, it is very flexible allowing any power sharing among the converters to be implemented, meanwhile the solutions in centralized and distributed controls to correct power sharing are designed for achieving one specific power sharing among the converters. The capability of the proposed secondary control to implement any power sharing allows the integration of any criteria for the power sharing, providing a high flexibility. For example, the secondary control can be combined with optimization problems, like the use of ESS contributing to the grid stability working in droop mode, meanwhile the secondary control optimizes its use in terms of cost. The proposed secondary control is also able to easily fix any reactive ac power sharing criteria, including active power loads that can contribute to the reactive power production if interfaced with a PEC, without additional droop control (Q/f droop is not required).

Secondly, since it requires only one calculation for operating point optimization, it has lower communication requirements and higher robustness against communication delays, high communication latency or loss of transmitted data compared to distributed and, especially, centralized secondary controls [9]. Decentralized secondary control does not require communications. However, considering communications infrastructure is always needed for coordination of distributed generation units during black start and microgrid real-time monitoring [8], the possibility of total lack of communications given by decentralized secondary control is not critical.

These differences are summarized in Table I.

This secondary control also provides the capability of compensating the voltage drop of virtual impedance techniques at the steady-state, [10]–[14]. As stated in [10] the virtual impedance can be used for many different purposes like active stabilization and disturbance rejection or, in the case of droop controllers, for making the line impedance more resistive/inductive, depending on the type of droop used.

However, this virtual impedance causes a voltage drop, that makes the effective total voltage drop greater, since the real output voltage of the converter is lower than the reference one (assuming that the converter is producing power). Some solutions can be found in the literature, like the use of a high-pass filter in the virtual impedance [11] to eliminate the effect of the virtual impedance in steady-state. However, this solution is only valid when the use of the virtual impedance is needed because of its transient effect (like the active stabilization aforementioned). When the steady-state effects of the virtual impedance are also needed, this solution is not valid. It is shown in this paper, how the designed secondary control can take into account this virtual impedance and eliminate the effect of its voltage droop. This is done by adding extra nodes to the optimum power flow calculation and selecting the physical connection of the converter, after the virtual impedance, to be the node having 1 p.u. voltage.

This paper extends the contributions in [15] by the same authors, adding the analysis of the power flow calculation convergence used in the proposed control, experimental validation of the proposed method and an example of how to take advantage of the proposed secondary control in optimization problems.

This paper is organized as follows. In Section II, the proposed hybrid microgrid topology and the power converters topologies are described. In Section III, the control strategy is explained, with a special focus in the proposed secondary control. Sections IV and V show the simulation and experimental results respectively. Section VI shows an example of how to integrate the proposed secondary control with optimization problems. Section VII presents the conclusions.

II. PROPOSED MICROGRID TOPOLOGY

The hybrid ac/dc network architecture [15] proposed in this paper is shown in Fig. 1 with the topologies of the converters in the shadowed blocks. The ac feeders and the dc lines (both ± 375 and 48 Vdc) are modeled as purely resistive lines, assuming a maximum voltage drop of 5 % at the end of the line for the rated power.

Being the lines purely resistive, if reactive power loads and references were set to 0, the ac part of the microgrid could be studied as if it was dc. Being the q-axis component of the voltages equal to 0 in steady-state, the d-axis component is equivalent to a dc voltage for the calculations.

For this reason, the analysis done in the paper starts with the dc case, since it is also a simplified study of the ac part. From dc solution, some modifications are done in order to include reactive power and possible non purely resistive impedances in the calculations for the ac complete solution.

As explained in Section I, virtual impedance can be used for different purposes, introducing an induced voltage drop. In this paper, virtual impedance is used for the converters in the ac feeders and is taken into account too for compensating its voltage drop.

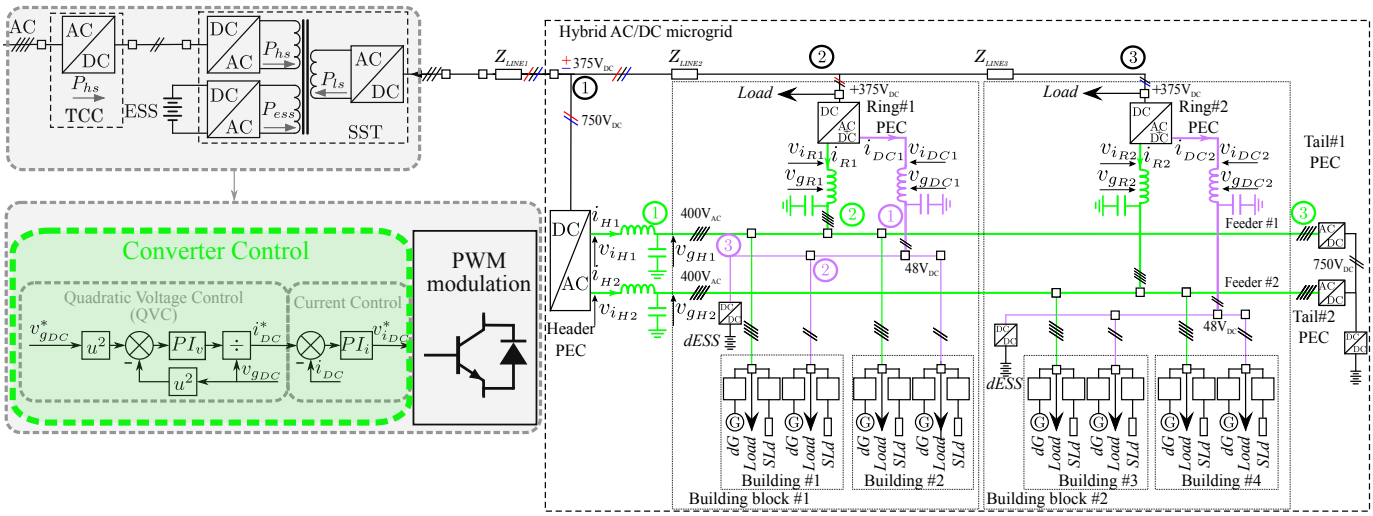

Fig. 1. Proposed system level grid infrastructure [15]. Shadowed blocks in the left side indicates the simplification of the SST connection as a dc/dc converter controlling the voltage.

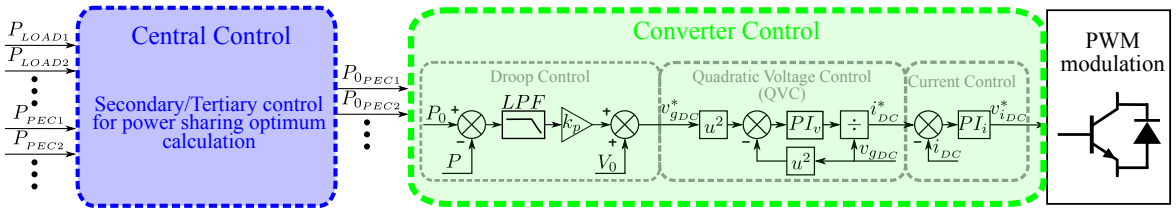

Fig. 2. General control diagram for converters in the 48 Vdc network. P_{LOAD_i} is the aggregate load connected to node i, P_{PEC_i} is the measured power output of the converter and $P0_{PEC_i}$ is the power offset for the converter connected to node i.

III. Coordinated control

As explained in the previous sections, the coordinate control of the power converters is done with a P/V droop control, both for the ac feeders and the 48 Vdc network.

This droop control acts as a primary control, making possible that all the converters which can deliver power, either coming from the connection to the main ac grid or from ESS, contribute to the power sharing.

The power sharing at the primary control level is achieved without requiring communication among the power converters. However, communication among them is used for upper level control, namely secondary and tertiary control for enhanced power sharing. This is later discussed in the paper.

A. ±375 *Vdc grid control*

In the ±375 Vdc grid, the SST provides connection to the mains supply and to the central ESS. In the present paper, this is simplified as a dc/dc converter connected to a dc voltage source since the focus is in the hybrid microgrid. This dc/dc converter controls the voltage difference between the positive and the negative bus (750 Vdc) as shown in Fig. 1.

Header PEC (HPEC), connected to node 1, is in charge of the dc bus balancing [16], due to its neutral point clamped topology, assuring that the voltage in both buses is 375 Vdc (one positive and one negative with respect to the neutral).

These two buses are distributed so that loads can be directly connected to these dc buses. They can be connected to either bus, so loads can be strongly unbalanced. Apart from that, Ring#1 PEC is connected to +375 Vdc bus and Ring#2 PEC is connected to −375 Vdc bus.

These two buses are distributed, so that loads can be directly connected to them. Due to the different loads at each of the buses (Ring#1 PEC at the +375 Vdc and Ring#2 PEC to the −375 Vdc bus respectively), they could become strongly unbalanced thus making much needed the balancing control implemented at the HPEC.

B. 48 *Vdc network control*

In Fig. 2 the control diagram for the 48 Vdc grid is shown. The control system is separated into two main blocks; 1) the internal converter control and 2) the central control. The internal control implements the voltage control using a quadratic approximation [17] and relies on a cascaded-architecture with an internal current controller. The references for the voltage control are given by a P/V droop. Connected to the internal control, the central controller provides the power offsets (P_0) to the different converters based on the secondary control, whose effect is to shift the droop curve.

The droop characteristic equation is shown in (1), where V is the resulting voltage from the droop control; k_p is the droop coefficient; P, the measured power output; P_0 and V_0

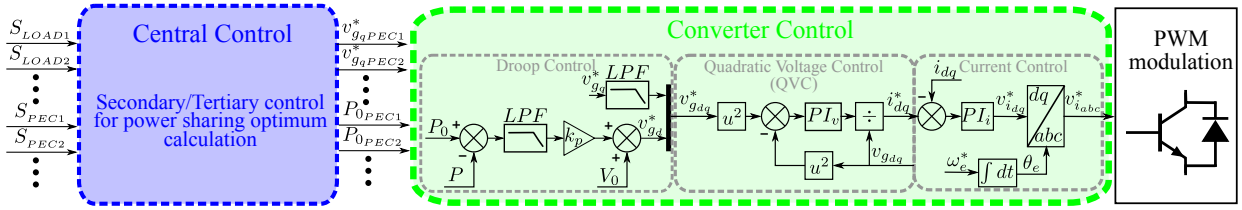

Fig. 3. General control diagram for converters in the ac feeder. S_{LOADi} is the aggregate load connected to node i, S_{PECi} is the measured power output of the converter and $P_{0_{PECi}}$ is the active power offset for the converter connected to node i. Both S_{LOADi} and S_{PECi} mean P and Q are required (being $S = P + jQ$).

the offset power and voltage (equal to rated voltage in the study case).

$$V = k_p(P_0 - P) + V_0 \tag{1}$$

C. 400 Vac feeder control

The general control scheme for the converters in the ac feeder is shown in Fig. 3, which is completely equivalent to the 48 Vdc network case except from the decomposition in the synchronous dq reference frame. Details about cross-coupling and feedforward terms shown in [17] are omitted due to space constraints. The reference for the d axis voltage control is given by a P/V droop. The central controller plays the same role as in the case of the 48 Vdc network. In here, also the q-axis voltage reference is provided to the different converters.

D. Secondary control

For the secondary control, a new strategy has been used. The idea consists on changing the P/V droop characteristics of each converter, by modifying the offset power P_0 in (1), so that they match the desired solution. For this paper, the chosen solution is to have a power sharing among the droop controlled converters proportional to each converter power rating and a voltage of 1 p.u. at a given specific node. In general, the output of the main converter of the corresponding grid is used as the 1 p.u. reference.

This secondary control is applied to the 400 Vac feeder and the 48 Vdc network. Considering the proposed grid topology in each case, the loads at each node and the reference output power of each converter, the power flow can be calculated, resulting in the voltage profile at each node considering one of the nodes is set to 1 p.u. For these calculations, only droop-controlled converters participating in the power sharing are taken into account as controllable converters, the remaining are seen as bidirectional loads.

The reference power output of each converter can be selected with different criteria. For the calculations presented hereafter, the sharing among the converters is proportional to the power rating of each converter. If any other criteria is used, this method could easily accommodate to it without further implications.

In this case, as shown in Fig. 1 both studied cases, the ac feeder or the 48 Vdc network, are radial networks, without rings inside. This eases the calculation of the power flow. Different grid topologies, including mesh and ring networks could also be considered, thus increasing the computational burden for the power flow calculations [18].

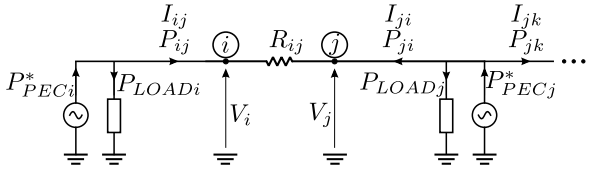

Fig. 4. Power flow diagram. P_{ij} (I_{ij}) is the power (current) flow from node i to j, P_{ji} (I_{ji}) from j to i and P_{jk} (I_{jk}) from j to k. P^*_{PECi}: reference power for converter at node i, P_{LOADi}: total connected load in that node and V_i: voltage in that node. R_{ij} is the equivalent impedance connecting node i and j (it should include both wires impedance in dc).

Calculations required for dc and ac case are very similar, but dc case is presented before, since it is simpler and more straightforward because it does not include reactive power. After presenting both cases, the possibility of including virtual impedance is presented too.

1) Secondary control in dc: Knowing the reference power and the voltage at each converter, obtained from the power flow, P_0 can be calculated so that the droop characteristic, whose equation is shown in (1), meets the requirements. The method is explained using network shown in Fig. 4.

In Fig. 5, the flowchart for the method is shown. Step 1 is for initialization, starting assuming no losses. Step 2 to 6 perform an iteration of the power flow. After step 6, a stop criterion is checked for deciding whether to stop or to continue with the next iteration, for a more precise calculation of the power flow solution. An analysis of power flow convergence is shown later in Subsection III-E. Step 7 calculates the offset power for each converter, P_{0PECi}, so that the droop curve of each converter matches the solution from the power flow, as shown in Fig. 6. This offset power is sent back to the converter control to modify their droop (see Fig. 2).

2) Secondary control in ac: The implementation of the secondary control in ac resembles the dc case but power (S, in this case), voltage, impedance (Z) and currents are complex magnitudes.

Fig. 7 show the corresponding calculations for ac. The only significant difference is in the last step. Since the droop is applied to P and V_d (real part of S and V complex vectors), the equation for calculating the active power offset relies on the real V component (d-axis), while imaginary (q-axis) component is sent as a direct reference to the converters.

Apart from the differences due to the use of complex variables in ac, the voltage drop for the dc case is calculated as $RI = R\dfrac{P}{V}$ meanwhile in ac it is $ZI = Z\dfrac{\overline{S}}{\sqrt{3}\cdot\overline{V}}$, because the ac network is three-phase.

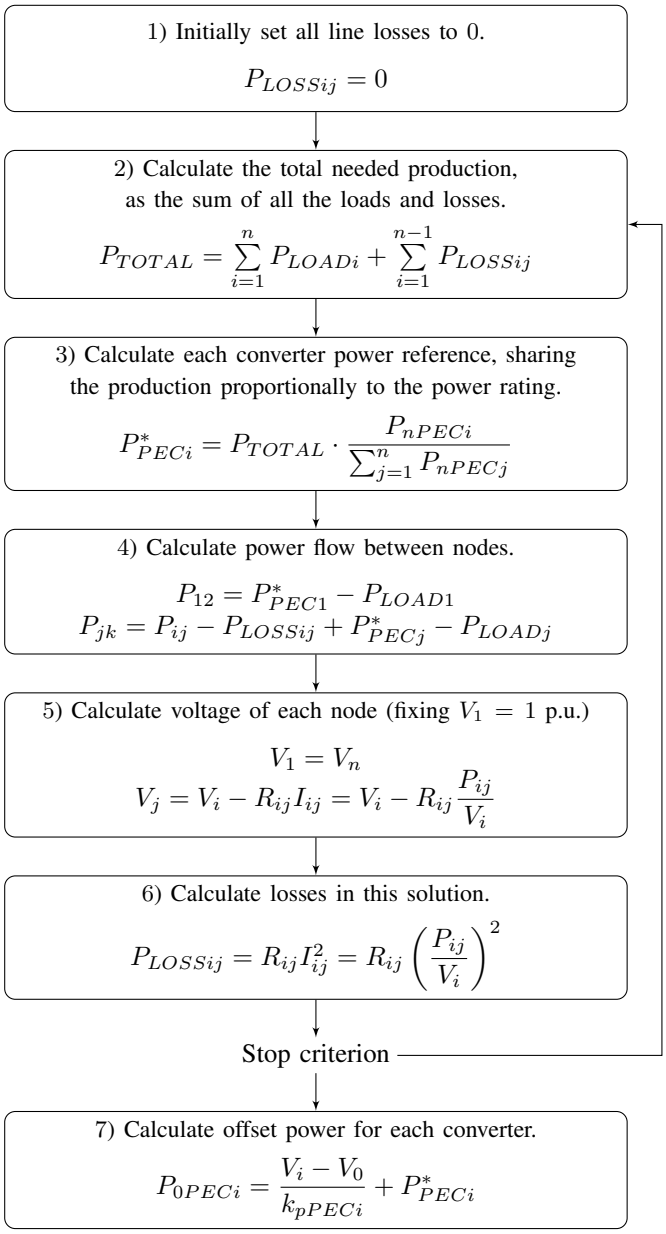

Fig. 5. Flowchart for secondary control in dc. i, j and k denote any three consecutive nodes.

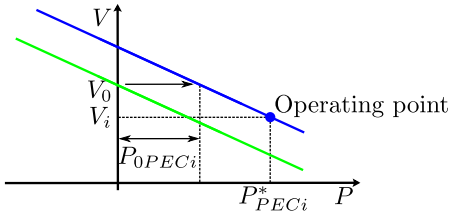

Fig. 6. Droop curve shift for fulfilling power flow solution. Green: base case with $P_{0PECi} = 0$ and blue: final solution.

3) Secondary control including virtual impedance: As explained in Section II, when virtual impedance is considered, the proposed secondary control allows for the compensation of the induced voltage drop. The compensation is achieved by adding virtual nodes to the power flow calculation shown in Fig. 7.

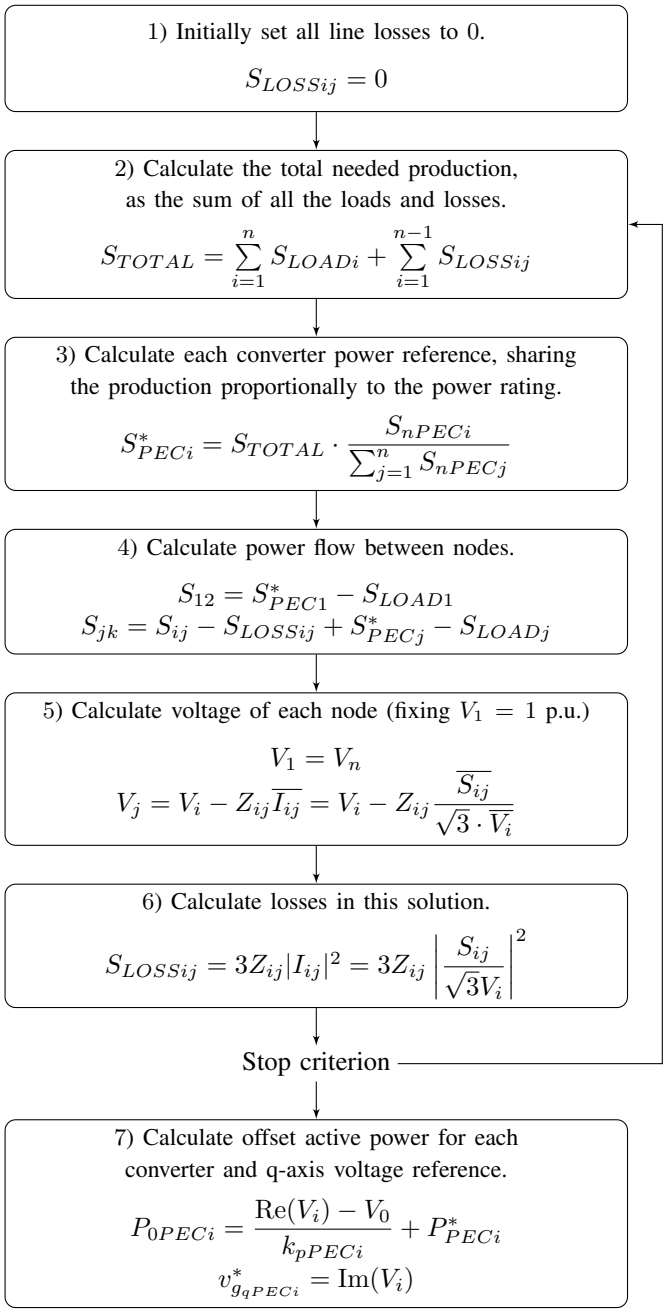

Fig. 7. Flowchart for secondary control in dc. i, j and k denote any three consecutive nodes. For obtaining a more compact expression, active and reactive power equations are presented in its complex form, so they are joint into one equation with $S = P + iQ$, using also $Z = R + iX$. $\overline{x}$, $\mathrm{Re}(x)$ and $\mathrm{Im}(x)$ are the conjugate, real part and imaginary part of a complex vector.

In the example shown in Fig. 7, voltage in physical node 1, V_1, is selected to be 1 p.u., obtaining this voltage at the physical connection of the PEC to that node. A virtual node is added before the virtual impedance voltage drop. This can be seen in Fig. 8 with an example of a circuit including virtual impedance, $Z_{vir,i}$. The voltage in the node in which each converter is physically connected is V_i and it is the one

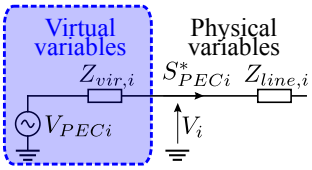

Fig. 8. Example of circuit including virtual impedance. V_i is the voltage at the physical connection of the corresponding PEC and $Z_{line,i}$, the coupling impedance. $Z_{vir,i}$ is the virtual impedance of the PEC and $V_{PEC,i}$, the (virtual) voltage before the voltage drop in the virtual impedance.

obtained from the power flow explained before. The voltage before the virtual impedance, $V_{PEC,i}$, can be obtained from V_i, adding the voltage drop in the virtual impedance. This calculation is shown in (2).

$$V_{PECi} = V_i + Z_{vir,i}\frac{\overline{S^*_{PECi}}}{\sqrt{3}\cdot\overline{V_i}} \tag{2}$$

The calculated V_{PECi} should be used instead of V_i in last step in Fig. 7. So in Fig. 8, the virtual voltage $V_{PEC,i}$ is the one used for the droop calculations, while V_i is the reference voltage for the physical node, achieving $V_1 = 1$ p.u.

The calculation presented in (2) is done considering a three-phase ac system, while extension to the dc case only requires to use real instead of complex variables for the impedance and power and without the $1/\sqrt{3}$ factor for the voltage drop calculation.

E. Power flow calculation convergence

The proposed secondary control is based on the calculation of the power flow solution. This power flow solution is an iterative process, thus an stop criteria is needed. It can be both a fixed number of iterations, a threshold for the difference of some calculated variables between consecutive iterations of the algorithm or a combination of both.

In this paper, for analyzing the convergence of the method, the difference between the losses obtained at the end of the iteration (step 6 in Fig. 5 and Fig. 7) and the ones calculated in the step before is used. When this difference is below a threshold, the solution can be considered precise enough.

The convergence time can be improved if instead of assuming zero losses in the first iteration, the losses in the situation prior to secondary control execution are used. This can be done simply by using the power production of each converter (P_{PECi}) for calculating the total needed production in step 2 for the first iteration. Using P_{PECi} instead of P_{LOADi} for this first iteration will make the losses of the previous situation to be included. Although P_{PECi} is not required for the rest of the algorithm, this is normally an information that the central controller can easily have.

To check the convergence, a simulation for the proposed microgrid is performed. The results are shown in Table II, where dc and ac cases are shown. The effect of using P_{PEC} for the first iteration is also included. It can be seen that the power flow converges in few steps, leading to an error below 0.8 ‰ in all the cases. The use of P_{PEC} for the initialization

TABLE II
ERROR FOR DIFFERENT NUMBER OF ITERATIONS (n) OF THE ALGORITHM. FIRST AND SECOND COLUMNS: DC NETWORK; THIRD AND FOURTH: AC FEEDER. FIRST AND THIRD COLUMNS: RESULTS USING P_{LOADi} FOR THE FIRST ITERATION; SECOND AND FOURTH COLUMNS: USING P_{PECi}.

n	dc: P_{LOAD}	dc: P_{PEC}	ac: P_{LOAD}	ac: P_{PEC}
1	0.78 ‰	0.17 ‰	2.34 ‰	0.21 ‰
2	0.17 ‰	0.17 ‰	0.18 ‰	0.18 ‰
3	0.17 ‰	0.17 ‰	0.18 ‰	0.18 ‰

TABLE III
CONVERTER PARAMETERS.

Converter	HPEC	RPEC-ac	RPEC-dc	dESS-PEC
S_n / P_n	7.5 kVA	3.75 kVA	1.25 kW	1.25 kW
k_p (p.u.)	0.1	0.1	0.05	0.05
f_c (Hz)	50	50	0.5	0.5

reduces the error of this first iteration, although no difference is seen from the second one onwards. For this paper, due to the fast convergence of the power flow solution, a fixed and small number of iterations (5) has been chosen for the stop criterion, although comparing the difference between losses calculated in consecutive iterations with a threshold would work similarly.

IV. SIMULATION RESULTS

The presented solution has been simulated using Matlab/Simulink. The complete hybrid microgrid is depicted in Fig. 1, including node numbers and code colors for the different sections: green for ac feeder; purple for 48 Vdc network; black for the ±375 Vdc buses.

In the ac feeder, nodes 1 and 2 are connected to the HPEC and to the ac output of the Ring PEC (RPEC-ac) respectively, by implementing a droop control strategy. Loads are connected to nodes 2 and 3, where the TPEC works in PQ mode. Both the HPEC and RPEC-ac have a virtual impedance of 5 times the line impedance in the ac feeder.

In the 48 Vdc, the dc output of the RPEC (RPEC-dc) works in droop control, together with a 1.25 kW dc/dc converter operating as a distributed ESS (dESS-PEC). A constant power load (CPL) is connected to node 2. In the ±375 Vdc grid, HPEC connected to node 1, is in charge of the dc bus balancing [16], while loads are connected both to 2 (positive dc bus) and 3 (negative dc bus). The details of the rated power of each converter and droop coefficients (k_p) are shown in Table III. Droop low pass filter (LPF) cutoff frequency are also shown. Cutoff frequency for dc is small because of the low communication speed in the experimental setup.

The simulation results are shown in Fig. 9. Before vertical lines marked with 1 (for 48 Vdc network) and 2 (ac feeder), the secondary control algorithm is disabled, thus having only a classical droop control. It can be seen the operation of the droop, which has two undesirable results. First, the power sharing among the converters is different from the desired one. In the ac feeder, the active power sharing ratio should be 2 : 1, proportional to their power ratings, but it is not even though the droop coefficient has the same per unit value. In ac, for the reactive power no droop is being used, so the sharing without secondary control is not controlled anyway

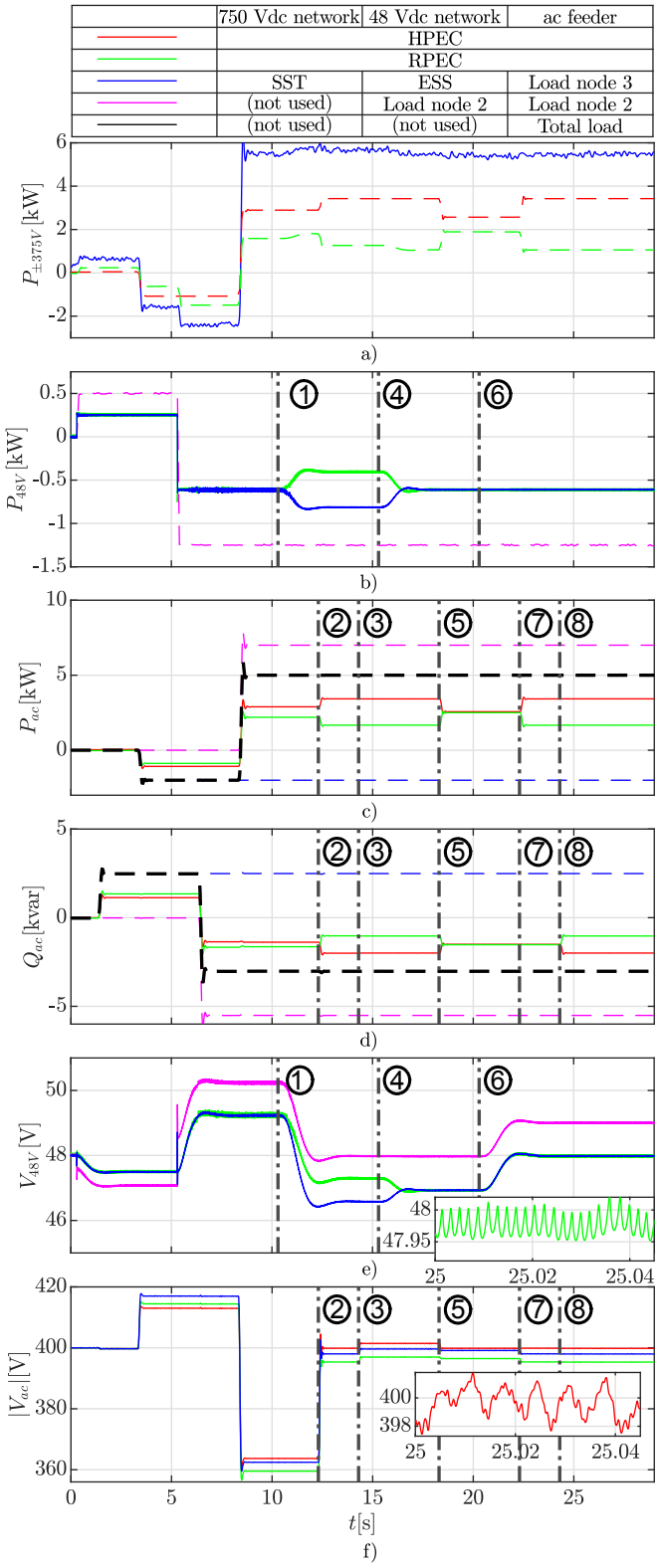

Fig. 9. Simulation results. a) Power in ±375 Vdc network. b) Power in 48 Vdc network. c) Active power in ac feeder. d) Reactive power in ac feeder. e) Voltage in 48 Vdc network, with a zoom to show the ripple. f) Filtered voltage in ac feeder (10 Hz LPF), zoom to show the ripple with unfiltered signal. For active/reactive power plots, load consumption is shown in dashed lines and converter production is shown in continuous lines. RPEC and HPEC are considered loads in the ±375 Vdc network.

and depends only on grid configuration and load demand. In the 48 Vdc network it matches the desired $1:1$ ratio because the network is completely symmetrical. Second, the droop causes a voltage deviation, making all the nodes far from 1 pu value (48 Vdc and 400 Vac respectively). Once the secondary control is enabled, these two effects are eliminated. Proposed secondary control algorithm is performed once per vertical line in Fig. 9. The sequence of power reference changes in the simulation are the following:

- At $t = 0.3$ s, power reference for CPL in node 2 of 48 Vdc network is set to 0.5 kW.
- At $t = 1.3$ s, reactive power reference for CPL in node 3 of ac feeder is set to 2.5 kvar.
- At $t = 3.3$ s, active power reference for CPL in node 3 of ac feeder is set to -2 kW.
- At $t = 5.3$ s, power reference for CPL in node 2 of 48 Vdc network is set to -1.25 kW.
- At $t = 6.3$ s, reactive power reference for CPL in node 2 of ac feeder is set to -5.5 kvar.
- At $t = 8.3$ s, active power reference for CPL in node 2 of ac feeder is set to 7 kW.

Sequence of changes in secondary control references (power sharing ratio and node with 1 pu voltage) is listed below. Changes in power sharing ratio are carried out by modifying step 3 in Fig. 5 and 7, with the desired proportion (the algorithm presented the case as if the desired proportion was proportional to the rated power).

1) At $t = 10.3$ s, secondary control is activated in 48 Vdc network, setting node 2 (load) to have 1 pu voltage (48 V) and sharing of power production among the two droop-controlled power electronic converters with $2:1$ ratio (ESS and RPEC output).
2) At $t = 12.3$ s, secondary control is activated in ac feeder, setting node 1 (HPEC) to have 1 pu voltage (400 V) and sharing of active and reactive power production among the two droop-controlled power electronic converters (HPEC and RPEC) proportional to their rated power ($2:1$ ratio). Is is worth to remark that 1 pu voltage is achieved in node 1, which has a converter with virtual impedance, being able to compensate the voltage drop in this virtual impedance.
3) At $t = 14.3$ s, 1 pu voltage reference in ac feeder is changed to node 3. The change is reversed in next update of secondary control in ac feeder.
4) At $t = 15.3$ s, power sharing ratio of converters in 48 Vdc network is set to $1:1$ ratio.
5) At $t = 18.3$ s, active and reactive power sharing ratio of converters in ac feeder is set to $1:1$ ratio.
6) At $t = 20.3$ s, 1 pu voltage reference in 48 Vdc network is changed to node 1 (RPEC output).
7) At $t = 22.3$ s, active power sharing ratio of converters in ac feeder is set back to $2:1$ ratio.
8) At $t = 24.3$ s, reactive power sharing ratio of converters in ac feeder is set back to $2:1$ ratio.

A. *Effect of grid parameters estimation mismatch*

In order to check the accuracy of the method under parameter estimation mismatches, a simulation has been performed forcing these estimation errors. The simulation has been done both for the ac feeder and the 48 Vdc network, in the same configuration explained previously in this section. For both cases, the network situation, including load consumptions, is exactly the same that there is at the end of the simulation shown in Fig. 9, only changing the situation of the load consumption in the ac feeder, where two nodes have loads. Apart from that, the only difference is in the performance of the secondary control.

The results are shown in Fig. 10. A variable error between ± 30 % has been included in the grid resistances estimation used for the secondary control. Both the ac feeder and the 48 Vdc network have the same configuration: R_{12} and R_{23} connecting nodes 1, 2 and 3 in a radial manner. For all the cases, the proposed variation for R_{12} estimation error has been added. Three different cases are considered for R_{23}: no error and same magnitude error as in R_{12} with same or opposite sign.

As commented before, the ac loads at the end of simulation shown in Fig. 9 are connected to nodes 2 and 3. In order to check which load configuration is more sensitive to estimation mismatches, two simulations have been performed. The sum of both loads in Fig. 9 is connected to one of the nodes. The results for the load connected to node 2 are the same for the three cases for the R_{23} error. This is a logical result, since if no load or PEC is connected to node 3, current does not flow in R_{23} and the estimation of that value has no effect. Similar results are obtained when all the load connected to node 3 with no error in R_{23}. Since no PEC is connected to node 3, for the secondary control, R_{23} and the node 3 load can be considered as a load connected to node 2, with a small variability due to the R_{23} losses. If the value of R_{23} is estimated properly, the losses are calculated exactly and there is no significant difference with the case where the load is directly connected to node 2.

In the results for the 48 Vdc network, it can be seen that the worst scenario is when the estimation has errors with opposite sign being the effect almost negligible for both power and voltage when the same sign estimation error occurs. The maximum deviation in absolute value is: 13.85 % for P_1 and P_3 and 0.35 % for v_1.

For the ac feeder, the worst scenario for active power and voltage occurs for same and opposite sign error respectively. For the reactive power, all the cases show almost identical results. The maximum deviation in absolute value is: 2.80 % for P_2, 5.51 % for Q_2 and 0.18 % for v_1. The errors for P_1 and Q_1 are in all cases smaller than those for P_2 and Q_2.

It can be seen that in all cases the error in terms of voltage is really small, meanwhile for all the other variables (active/reactive power), the maximum error in all the scenarios is 13.85 %. Considering that this error occurs for a very significant error (30 %), the method can be considered robust

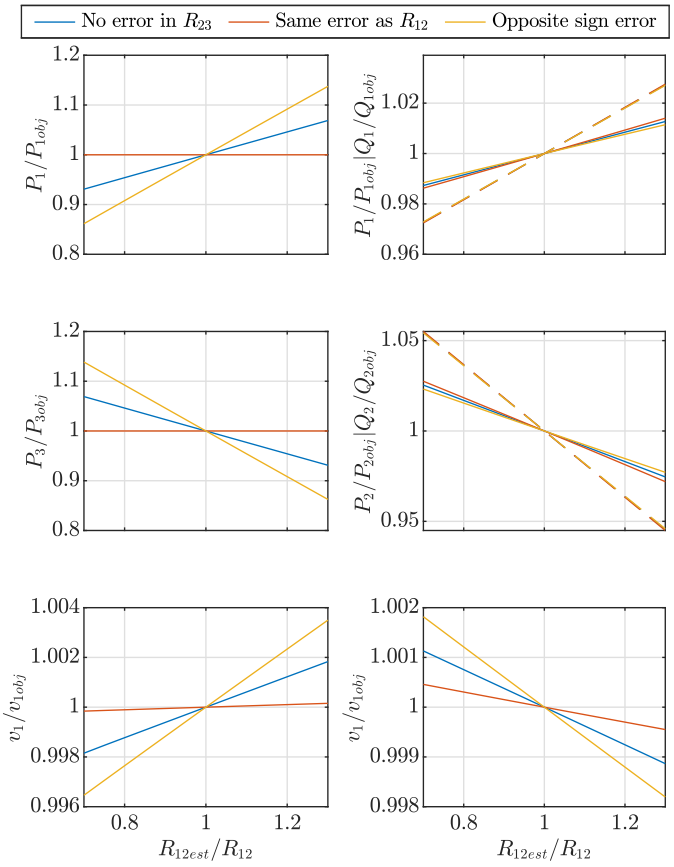

Fig. 10. Estimation mismatch simulation results. Left column: dc network; right column: ac feeder. First two rows indicate both PECs power production compared to the reference one for the secondary control (two PECs in each case, dc and ac; for ac, dashed lines indicate reactive power). Third row indicates deviation in the voltage in the node whose voltage is chosen to have 1 pu voltage.

enough referring to parameters estimation mismatches. Taking into account that these important errors only appear for power sharing and not for voltage magnitude, the method can be considered as a valid alternative to other secondary control alternatives, which normally correct the voltage deviation of the droop controllers but have no capability of varying the power sharing in a flexible way.

The application of this secondary control is thought for microgrids, coordinated by a central controller with access to measurements in the different nodes. In this scenario, a proper estimation of all the required parameters can be worthy for multiple reasons, including an optimum operation of the microgrid (like losses optimization). Online parameter estimation methods are found in the literature and some of them use the same variables required for the secondary control, to perform an inverse power flow problem, estimating impedances from current and voltages in the different nodes [19]. This strategy for online parameter estimation is very convenient to be run in parallel with the secondary control, when offline estimation is not possible.

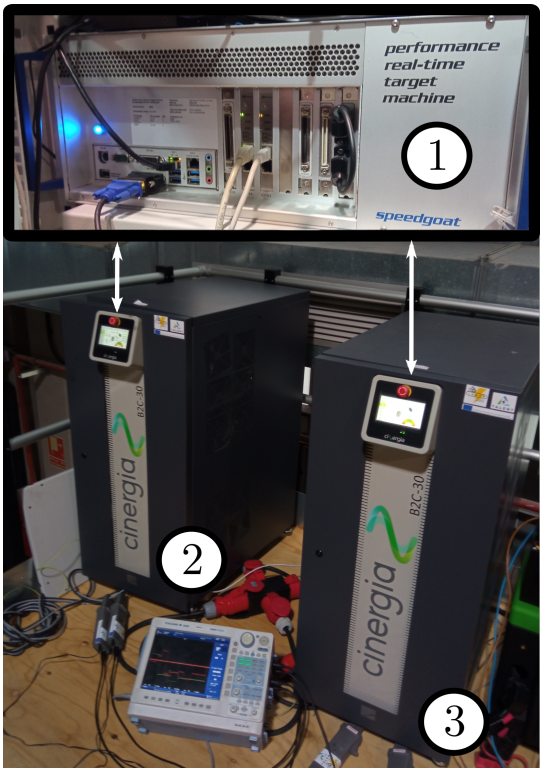

Fig. 11. Setup for experimental validation. Speedgoat real-time simulator (1): implements the ac feeder and controls two Cinergia B2C-30 converters, one for the 750 Vdc network (2) and the other for the 48 Vdc network (3). White arrows indicate Modbus/TCP communication channels for the real-time simulator to send references to and receive measurements from the converters.

V. Experimental validation

The proposed method has been validated experimentally with the setup shown in Fig 11. The microgrid shown in Fig. 1 is partially implemented. The ±375 Vdc grid is simplified to a unipolar 750 Vdc bus and only one ac feeder and one 48 Vdc network are used.

The two Cinergia B2C-30 converters shown in Fig. 11 are controlled through the Speedgoat real-time simulation platform, sending power references to outputs operating as constant power loads and voltage references to the droop-controlled converters, with the droop calculations inside the real-time simulator. Real measurements from the converter outputs, using Modbus/TCP communications, are fed back for the calculation inside Speedgoat. The ac feeder is implemented in the real-time simulator. The interconnection of the ac feeder and the 48 Vdc network with the 750 Vdc bus is implemented as a load in the 750 Vdc, whose demand is updated with the production of the corresponding converter: RPEC in 48 Vdc network (real power measurements) and RPEC and HPEC in the ac feeder (real-time simulation data).

In Fig. 12, the results from the experimental setup validation are shown, with the same sequence of changes in load and secondary control references explained in Section IV for the Simulink simulation. It can be seen that the experimental results agree with the simulated ones, thus validating the proposed secondary control.

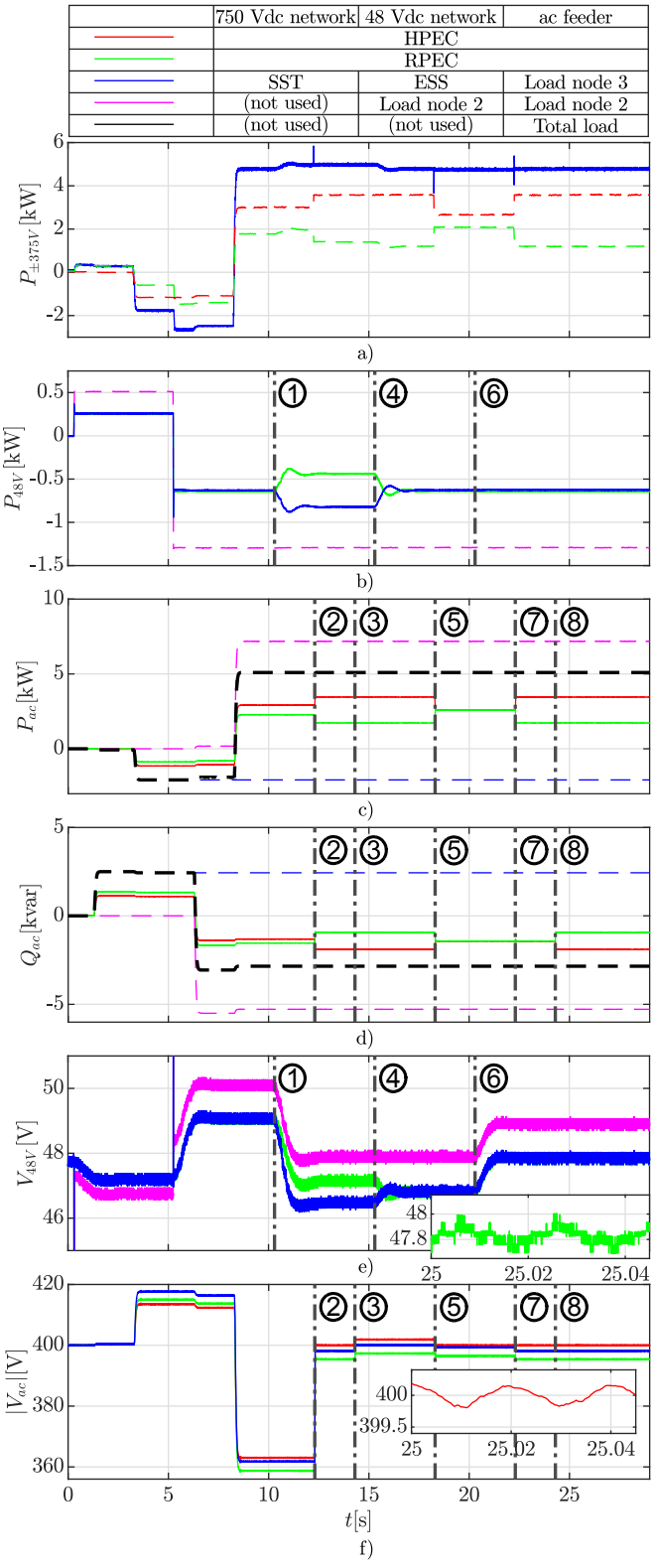

Fig. 12. Experimental results. a) Power in ±375 Vdc network. b) Power in 48 Vdc network. c) Active power in ac feeder. d) Reactive power in ac feeder. e) Voltage in 48 Vdc network, with a zoom to show the ripple. f) Voltage in ac feeder, with a zoom to show the ripple. For active/reactive power plots, load consumption is shown in dashed lines and converter production is shown in continuous lines. RPEC and HPEC are considered loads in the ±375 Vdc network.

VI. Combination with power sharing optimization criteria

In the previous sections, the power sharing was determined as a constant proportion between both converters production.

In this section, this power sharing selection is chosen for optimizing a given cost function, thus illustrating the versatility of the proposed method.

Optimization problems including power flows normally require iterative processes, for the same reason power flow solutions are normally iterative. For this reason, the iterative process explained in Fig. 5 can be used for calculating the optimization problem at the same time the power flow is being solved, being the study case for the optimization problem is in dc.

The cost function to be minimized is (3), where P_l are the losses in the network, P_{load} and P_b the power consumed by the load and the battery used as ESS, C_0 is the cost of energy at the moment of optimization and C_1 is the expected cost of energy in a future moment of the day.

$$C = C_0 P_g - C_1 P_b = C_0(P_l + P_b + P_{load}) - C_1 P_b \quad (3)$$

This cost function represents the cost per unit time of the consumed energy, $C_0 P_g = C_0(P_l + P_b + P_{load})$, minus the expected revenues from the energy stored in the battery for a future sell, $C_1 P_b$. P_b is considered with load convention, so a positive value means it is being charged, thus having a positive future revenues (reducing cost). The two costs, C_0 and C_1 are thought for tariff with hour discrimination, in which the price for peak and valley moments of the day can be known and used for estimating the possible earns with battery usage.

For the losses calculation, only the losses in the lines in the 48 Vdc network are considered, neglecting the losses in PEC and assuming RPEC is directly connected to the grid (so grid variables from now on indicate RPEC output). The same procedure applied here can be used for more complete losses calculation, as it can be used including other parts of the grid, but it complicates the problem and is considered as future work out of the scope of the paper.

Losses can be calculated as shown in (4), where R is the resistance of the line connecting to the load, indicating subscript g and b grid or battery side, and V is the voltage at grid/battery PEC output.

$$P_l = \frac{R_b}{V_b^2} P_b^2 + \frac{R_g}{V_g^2} P_g^2 = \frac{R_b}{V_b^2}(1-r)^2 P_T^2 + \frac{R_g}{V_g^2} r^2 P_T^2 \quad (4)$$

Where P_g and P_b are expressed as a function of total production that the battery and grid must share ($P_T = P_l + P_{load}$): $P_g = r P_T$ and $P_b = (1-r)P_T$, being r the proportion of this demand supplied by the grid (P_{TOTAL} in Fig. 5).

Substituting (4) in (3) and differentiating with respect to r, the condition for the minimum of the function is obtained, as shown in (5).

$$C' = C_0 \frac{2R_b}{V_b^2}(r-1)P_T^2 + C_0 \frac{2R_g}{V_g^2} r P_T^2 - (C_1 - C_0)P_T = 0 \quad (5)$$

Defining $B_x = 2P_T R_x / V_x^2$ (where x can be either g or b) and $C_{diff} = (C_1 - C_0)/C_0$, and dividing by $P_T C_0$ condition shown in (5) can be rewritten as shown in (6).

$$B_b(r-1) + B_g r - C_{diff} = 0 \rightarrow r = \frac{B_b + C_{diff}}{B_b + B_g} \quad (6)$$

Losses (used for obtaining P_T) and voltage in each node are assumed as constants for this calculation, although they depend on the solution. This means that the optimum will not be found with one single calculation, since the value of r, whose optimum is being calculated, is affecting the parameters needed for its calculation. However, this optimum calculation can be added to the iterative nature of power flow algorithms (used in the proposed secondary control), recalculating the constants for every iteration. This process does not fully guarantee the convergence to the optimum point, but it will be seen that the deviation is generally small.

Due to this possible deviation from the optimum solution, and in order to make the method valid for more complex problems in which an expression for r might be impossible to obtain, another method for the optimum calculation is proposed. For this method, the iterations of the secondary control are done with steps in the different values of r, doing a sweep among the possible values. For every value of r, the cost function is calculated. If the calculated cost is minimum compared to the previous ones, the value of the cost function is updated to be used in the next steps. The value of the outputs of the secondary control (P_{0PECi} and, in the case of ac, also $v^*_{g_{qPECi}}$) is also stored to avoid recalculating the power flow after the sweep has finished. The explained Sweep Optimization method is shown in Fig. 13.

Since the steps in r are going to be relatively small, it can be considered that the power flow for each value of r converges in only one iteration, because it is starting from a similar solution. This way, the iterative nature of the power flow solution and the optimization problem is combined.

These two alternatives, which from now on are going to be referred as Optimum Calculation and Sweep Optimization, are going to be compared in order to check its effectiveness.

A. Simulation validation

The cost optimization problem presented in this paper is a simple case with a reduced version of the grid infrastructure presented in Fig. 1, with only one of the 48 Vdc networks.

The configuration of the study case network is the same used for Sections IV and V, with the RPEC connected to node 1, the ESS to node 3 and load to node 2. The load consumption is fixed to 1.25 kW for all the results presented here.

For validating the proposed optimization algorithm, a simulation has been carried out. For the same network situation, the value of r is varied in order to obtain the cost function for a given range. This is similar to the Sweep Optimization, but

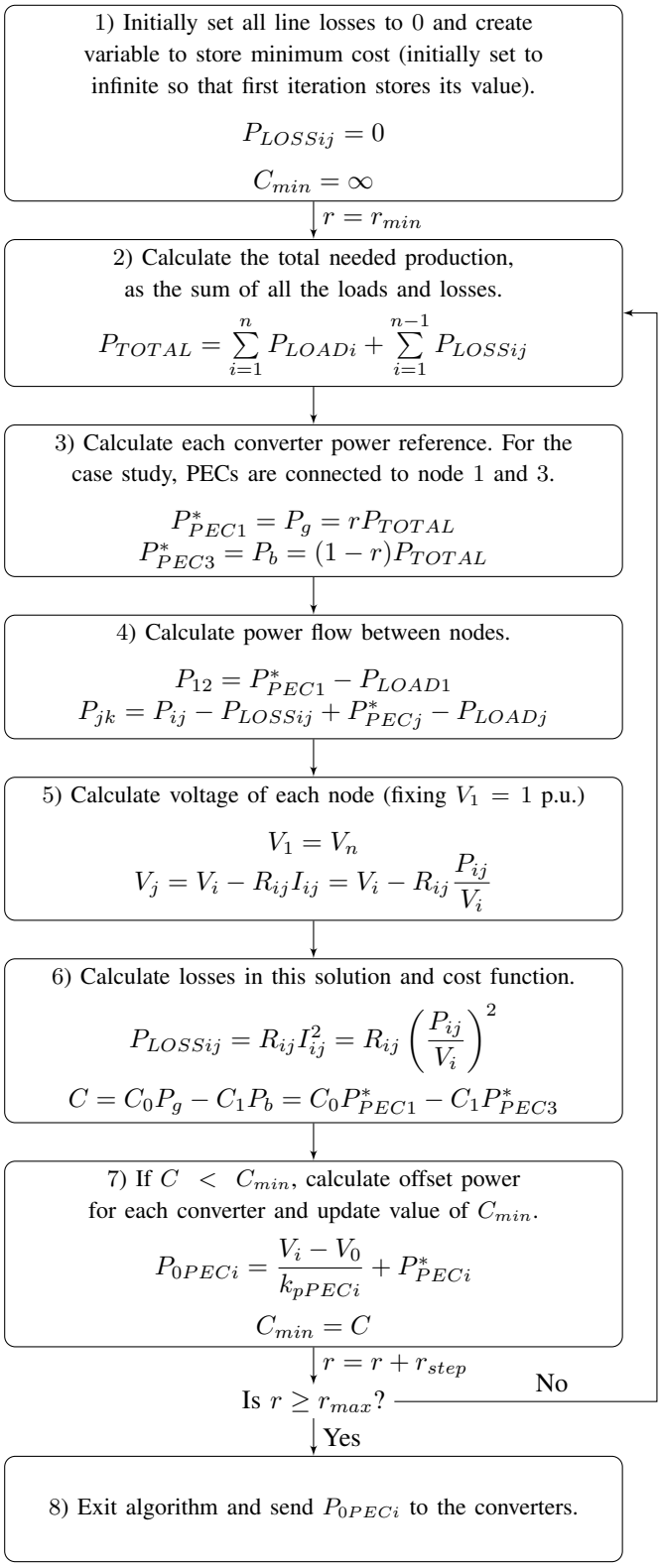

Fig. 13. Flowchart for secondary control with cost optimization in dc. i, j and k denote any three consecutive nodes. r_{min} and r_{max} are the minimum and maximum value of r for the sweep, and r_{step} is the step in r between iterations.

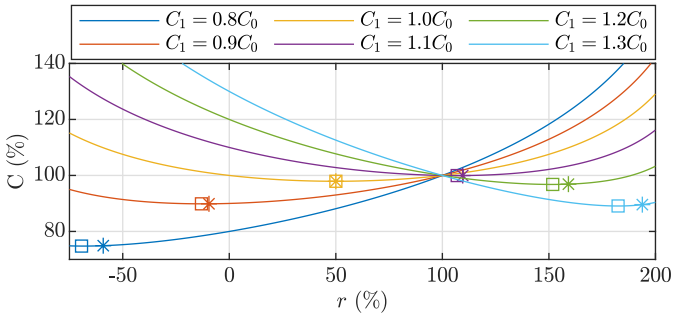

Fig. 14. Simulation results for different values of future energy cost (C_1) with respect to present value (C_0). r is the proportion of total load supplied by the grid connection and C is the expected cost compared to the case with no ESS ($r = 100$ %). Asterisks mark the position of the Optimum Calculation, meanwhile squares mark the minimum obtained by Sweep Optimization. Minimum values of C and r for each curve and values obtained with both methods for optimization are shown in Table IV.

TABLE IV
MINIMUM VALUE OF COST FUNCTION FOR DIFFERENT VALUES OF C_1 AND VALUES OBTAINED BY BOTH METHODS FOR OPTIMIZATION.

	Real value		Opt. Calculation		Sweep Opt.	
	r (%)	C (%)	r (%)	C (%)	r (%)	C (%)
$C_1 = 0.8C_0$	−68.5	74.8	−59.1	74.9	−69.3	74.8
$C_1 = 0.9C_0$	−12.5	89.9	−9.5	89.9	−13.1	89.9
$C_1 = 1.0C_0$	50.0	97.9	50.0	97.9	50.0	97.9
$C_1 = 1.1C_0$	106.9	100.0	109.5	100.0	107.0	100.0
$C_1 = 1.2C_0$	151.3	96.8	159.1	96.9	151.8	96.8
$C_1 = 1.3C_0$	182.5	89.1	193.8	89.6	182.5	89.1

in this case the secondary control shown in Fig. 5 is executed for each value of r during the simulation, the output of the secondary control for each value is sent to the converters and the cost function is obtained with the real values of P_g and P_b measured in the simulation. In the Sweep Optimization, the cost function is calculated in the algorithm, and the secondary control reference is sent to the PEC only when the sweep is finished.

The results can be seen in Fig. 14. Minimum values of cost (C) for each curve and corresponding value of r, together with values obtained with both methods for optimization are shown in Table IV. For Sweep Optimization a step of 1% for r has been used.

It can be seen that the error in the value of r for the Optimum Calculation is significant in some cases (up to 11.3 % in the worst case). Meanwhile, for Sweep Optimization, is always smaller than 1 %. However, in both methods, the obtained cost is really close to the actual minimum, with a maximum deviation of 0.5 % and less than 0.1 % for Optimum Calculation and Sweep Optimization respectively.

This indicates that the deviation in the Optimum Calculation from the actual minimum is not important, since although it can be significant in terms of the chosen r value, the obtained cost is close to the minimum one. This makes that this method is more suitable for the proposed scenario, since less iterations will be required. However, the validity of the Sweep Optimization method is also proved as an alternative for more complex problems in which the value of r minimizing the

cost function cannot be directly calculated. This could be the case of considering efficiency curves in PECs, more than one interconnected networks or multi-variable optimization (for example, if the sharing is between three instead of two PECs, adding one degree of freedom).

VII. Conclusions

This paper has shown an approach for the sharing control scheme in a hybrid ac/dc microgrid. The proposed method enables the different converters to contribute to the power sharing by a droop control implementation. The proposed secondary control eliminates the voltage deviation due to the droop characteristic. It also eliminates the voltage droop caused by the virtual impedance.

The proposed secondary control applied in ac allows the reactive power sharing among the converters with no specific droop control. This also eases the integration of converters which are seen as active power loads, but whose reactive power can be controlled to contribute to the sharing, as it can be the case of a converter feeding a load or a STATCOM. All the droop-controlled converters can achieve any active/reactive power production, thus achieving different power sharing scenarios, including shared conditions among the different networks in the hybrid microgrid if the secondary control of these different networks is coordinated. The proposed method has been validated both in simulation and in an experimental setup.

The secondary control is also flexible, allowing to introduce any criteria for the power flow solution, like any method for deciding the power sharing among the converters (minimize losses, saturation of converters for its rated power,...) or the possibility of easily changing the node whose voltage is fixed to 1 p.u. This flexibility has been proven with a simplified optimization problem, using the secondary control combined to the minimization of a cost function. Two alternatives were presented and validated through simulation, both with similar performance in terms of obtained cost. Cost Optimization approach is more suitable for simpler problems that can be solved analytically, whereas Sweep Optimization is a better option under complex scenarios. This could be the case of considering efficiency curves in PECs, more than one interconnected networks or multi-variable optimization.

References

[1] P. Wang, L. Goel, X. Liu, and F. H. Choo, "Harmonizing AC and DC: A Hybrid AC/DC Future Grid Solution," *IEEE Power and Energy Magazine*, vol. 11, no. 3, pp. 76–83, May 2013.

[2] P. Fairley, "DC Versus AC: The Second War of Currents Has Already Begun [In My View]," *IEEE Power and Energy Magazine*, vol. 10, no. 6, pp. 104–103, Nov 2012.

[3] A. Bindra, "Projecting the Evolution of Power Electronics: Highlights from FEPPCON VIII," *IEEE Power Electronics Magazine*, vol. 3, no. 1, pp. 32–44, March 2016.

[4] C. Marnay, H. Aki, K. Hirose, A. Kwasinski, S. Ogura, and T. Shinji, "Japan's Pivot to Resilience: How Two Microgrids Fared After the 2011 Earthquake," *IEEE Power and Energy Magazine*, vol. 13, no. 3, pp. 44–57, May 2015.

[5] J. Rocabert, A. Luna, F. Blaabjerg, and P. Rodríguez, "Control of Power Converters in AC Microgrids," *IEEE Transactions on Power Electronics*, vol. 27, no. 11, pp. 4734–4749, Nov 2012.

[6] J. W. Simpson-Porco, Q. Shafiee, F. Dörfler, J. C. Vasquez, J. M. Guerrero, and F. Bullo, "Secondary Frequency and Voltage Control of Islanded Microgrids via Distributed Averaging," *IEEE Transactions on Industrial Electronics*, vol. 62, no. 11, pp. 7025–7038, 2015.

[7] P. Wang, X. Lu, X. Yang, W. Wang, and D. Xu, "An Improved Distributed Secondary Control Method for DC Microgrids With Enhanced Dynamic Current Sharing Performance," *IEEE Transactions on Power Electronics*, vol. 31, no. 9, pp. 6658–6673, 2016.

[8] Y. Khayat, Q. Shafiee, R. Heydari, M. Naderi, T. Dragičević, J. W. Simpson-Porco, F. Dörfler, M. Fathi, F. Blaabjerg, J. M. Guerrero, and H. Bevrani, "On the secondary control architectures of ac microgrids: An overview," *IEEE Transactions on Power Electronics*, vol. 35, no. 6, pp. 6482–6500, 2020.

[9] Q. Shafiee, J. M. Guerrero, and J. C. Vasquez, "Distributed secondary control for islanded microgrids—a novel approach," *IEEE Transactions on Power Electronics*, vol. 29, no. 2, pp. 1018–1031, 2014.

[10] X. Wang, Y. W. Li, F. Blaabjerg, and P. C. Loh, "Virtual-Impedance-Based Control for Voltage-Source and Current-Source Converters," *IEEE Transactions on Power Electronics*, vol. 30, no. 12, pp. 7019–7037, 2015.

[11] Z. Liu, S. Ouyang, and W. Bao, "An improved droop control based on complex virtual impedance in medium voltage micro-grid," in *2013 IEEE PES Asia-Pacific Power and Energy Engineering Conference (APPEEC)*, 2013, pp. 1–6.

[12] A. Micallef, M. Apap, C. Spiteri-Staines, and J. M. Guerrero, "Performance comparison for virtual impedance techniques used in droop controlled islanded microgrids," in *2016 International Symposium on Power Electronics, Electrical Drives, Automation and Motion (SPEEDAM)*, June 2016, pp. 695–700.

[13] A. D. Paquette and D. M. Divan, "Virtual Impedance Current Limiting for Inverters in Microgrids With Synchronous Generators," *IEEE Transactions on Industry Applications*, vol. 51, no. 2, pp. 1630–1638, 2015.

[14] J. He and Y. W. Li, "Analysis, Design, and Implementation of Virtual Impedance for Power Electronics Interfaced Distributed Generation," *IEEE Transactions on Industry Applications*, vol. 47, no. 6, pp. 2525–2538, 2011.

[15] C. Gómez-Aleixandre, A. Navarro-Rodríguez, G. Villa, C. Blanco, and P. García, "Sharing control strategies for a hybrid 48v/375v/400vac ac/dc microgrid," in *2020 IEEE Energy Conversion Congress and Exposition (ECCE)*, 2020, pp. 3900–3907.

[16] C. Wang, Z. Li, X. Si, and H. Xin, "Control of neutral-point voltage in three-phase four-wire three-level NPC inverter based on the disassembly of zero level," *CPSS Transactions on Power Electronics and Applications*, vol. 3, no. 3, pp. 213–222, Sep. 2018.

[17] A. Navarro-Rodríguez, P. García, R. Georgious, and J. García, "Adaptive Active Power Sharing Techniques for DC and AC Voltage Control in a Hybrid DC/AC Microgrid," *IEEE Transactions on Industry Applications*, vol. 55, no. 2, pp. 1106–1116, March 2019.

[18] R. Chai, B. Zhang, J. Dou, Z. Hao, and T. Zheng, "Unified Power Flow Algorithm Based on the NR Method for Hybrid AC/DC Grids Incorporating VSCs," *IEEE Transactions on Power Systems*, vol. 31, no. 6, pp. 4310–4318, 2016.

[19] K. Gajula, L. K. Marepalli, X. Yao, and L. Herrera, "Recursive least squares and adaptive kalman filter based state and parameter estimation for series arc fault detection on dc microgrids," *IEEE Journal of Emerging and Selected Topics in Power Electronics*, pp. 1–1, 2021.

Carlos Gómez-Aleixandre (S'19) received the B.Sc. degree in electrical engineering and the B.Sc. degree in industrial electronic and automatic engineering from the University of Oviedo, Gijón, Spain, in 2015 and 2018, respectively. He received the M.Sc. degree in sustainable transportation and electrical power systems from the University of Oviedo, University of Nottingham, Sapienza Università di Roma and Instituto Superior de Engenharia de Coimbra in 2017. He is currently working toward the Ph.D. degree in electrical engineering with the LEMUR Research Team, University of Oviedo.

He has coauthored 2 IEEE journals and 7 IEEE international conference papers. His research interests include microgrids, coordinated control, and modeling and control of islanded and grid-connected converters

Mr. Gómez-Aleixandre received a Spanish Predoctoral Grant for the formation in university teaching (Formación de Profesorado Universitario) in 2017.

Ángel Navarro-Rodríguez (S'15-M'20) is "Cum Laude" Ph.D in Energy and Process Control. He received the B.Sc. degree in Telecommunications Engineering with honours from the University of Castilla La-Mancha, Spain in 2012, the M.Sc. degree in Electrical Energy Conversion and Power Systems, and the Ph.D. degree in Energy and Process Control from the University of Oviedo, Spain, in July 2014 and June 2019, respectively, granted by the government of Principado de Asturias. Nowadays, he is an Assistant Professor in the Department of Electrical, Electronics, Comunications, and Systems Engineering in the University of Oviedo since October 2019. In 2016/17 he was a Visitor Researcher with the PEMC Research Group in The University of Nottingham, U.K.

He has authored or co-authored 8 IEEE journals and more than 20 IEEE conferences, with a 7 h-index. He received the Outstanding Young EPE Member Award in 2018 and the University of Oviedo Outstanding Ph.D. Thesis Award in 2020. He is part of the LEMUR research group in the University of Oviedo since July 2014 and his current research interests include microgrids control and modelling, grid-tied converters, energy storage systems, control systems applied to electrical energy conversion, sustainable transportation and electric traction, power quality and renewable energies integration.

Geber Villa received the B.Sc. degree in electronics and control engineering, the M.Sc. degree in electrical energy conversion and power systems, and the M.Sc. degree in industrial engineering from the University of Oviedo, Gijón, Spain, in 2011, 2016, and 2017, respectively. He is currently working toward the Ph.D. degree in electrical engineering with the LEMUR Research Team, University of Oviedo.

He has coauthored several IEEE international conference and journals papers. His research interests include analysis and control of power converters, energy storage systems, and microgrids.

Mr. Villa received the Spanish National Award for the Outstanding Graduate of the Year in 2014 and 2021, and a Spanish Predoctoral Grant for the formation in university teaching (Formación de Profesorado Universitario) in 2017.(S'17) received the B.Sc. degree in electronics and control engineering, the M.Sc. degree in electrical energy conversion and power systems, and the M.Sc. degree in industrial engineering from the University of Oviedo, Gijón, Spain, in 2011, 2016, and 2017, respectively. He is currently working toward the Ph.D. degree in electrical engineering with the LEMUR Research Team, University of Oviedo.

Cristian Blanco (S10'-M'16) was born in Villablino, Leon, Spain. He received a B.S Degree in Telecommunications Engineering, a M.S. degree, and a PhD in Electrical Engineering from the University of Oviedo, Gijon, Spain, in 2010, 2011, and 2015 respectively.

In 2011, he was awarded a fellowship of the Personnel Research Training Program funded by the Regional Ministry of Education and Science of the Principality of Asturias. From Sep. 2012 to Feb. 2013 he was a PhD Guest at Aalborg University (Denmark). From Jul. to Dec. 2019 he was Visiting Faculty at the University of British Columbia (Canada). He is currently Associate Professor with the Department of Electrical, Computer, and Systems Engineering (University of Oviedo). At the same time, he works with the LEMUR research group; his research capabilities include modeling and control of islanded and grid-connected converters including storage systems, synchronization, islanding detection and power quality, microgrids and digital signal processing.

Dr. Blanco was the recipient of an IEEE Energy Conversion Congress and Exposition second prize paper award in 2013. At the same time, he received the University of Oviedo Outstanding Ph.D. Thesis Award in 2016.

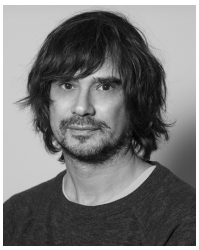

Pablo García was born in Luanco, Asturias, Spain. He received a M.S. degree, and a PhD in Electrical Engineering from the University of Oviedo, Gijon, Spain, in 2001 and 2006 respectively.

From 2002 to 2006 he was awarded with a fellowship for the national research and training program by the Ministry of Science and Technology in Spain. In 2004 he was a visiting Scholar at the University of Wisconsin-Madison, USA. In 2013 he was a visiting Scholar at The University of Nottingham, UK. He is currently a Full Professor within the Department of Electrical, Electronics, Communications and Systems Engineering, University of Oviedo. From 2022 he works with the Spanish Research Agency as the manager for international projects in the Energy and Transport division area. He is a member of the LEMUR research group. His research interest include control of grid-tied power converters for distributed resources integration and particularly for the control of grid-tied battery energy storage systems, parameter estimation, optimization of distributed resources and digital signal processing for real-time embedded systems. He is the co-author of near 40 journal papers and 80 conference papers. He has been the Principal Investigator of 50 projects with companies, 1 European H2020 and 4 national funded projects. He is the co-founder of the ENFASYS startup, focused on the development of solutions for the integration of energy storage and collaborative self-consumption applications.

He was a recipient of the 2005 IEEE Transactions on Industry Applications, Third Place Prize Paper Award, three IEEE Industry Applications Society Conference prize paper awards in 2006, 2010 and 2016, respectively and one EPE Conference Award in 2018.